Effect of Electromagnetic Field on the Microstructure and Mechanical Properties of the Dissimilar 2205/316L Welded Joint

S. L. Hernández-Trujillo, V. H. López-Morelos, R. García-Hernández, M. A. García-Rentería, A. Ruiz-Marines and J. A. Verduzco-Martínez

Introduction

Welding of dissimilar stainless steels has been increasingly considered in many applications in the petrochemical, pulp and paper, chemical and oil industries as well as in power and desalination plants due to several benefits including reduction of material costs and improvements in design and components [1–3]. The practice of welding dissimilar materials represents a major challenge owing to the differences in physical, mechanical and metallurgical properties and the use of a filler that may does not match the chemical composition of any of the parent plates. Thus, a deeper understanding of the behavior of dissimilar welded joints is needed and assessment of their performance is being carried out to establish the relative benefits of welding two different stainless steels based on cost, weight, mechanical properties and corrosion resistance to fulfill safety and structural requirements. Proper selection of the filler metal is an important aspect to evaluate in the design of a dissimilar weld for a satisfactory performance in service [4].

On their own, ASS and DSS are widely used in many engineering applications. These steels present excellent combination of corrosion resistance, ductility, toughness and mechanical strength. Weldability studies of DSSs and ASSs have been extensively carried out, but only a few studies have been reported on dissimilar welds between these alloys [2–4]. ASS grade 316L is one of the most popular stainless steels due to its excellent weldability and reduced susceptibility to

S. L. Hernández-Trujillo (✉) · V. H. López-Morelos · R. García-Hernández · A. Ruiz-Marines · J. A. Verduzco-Martínez
Instituto de Investigación en Metalurgia y Materiales, Universidad Michoacana de San Nicolás de Hidalgo, Edificio "U", Ciudad Universitaria, Morelia, Michoacán, Mexico
e-mail: saullht@yahoo.com.mx

M. A. García-Rentería
Facultad de Metalurgia, Universidad Autónoma de Coahuila, Carretera 57 Km 5, Los Bosques, 25710 Monclova, Coah, Mexico

R. R. Ambriz et al. (eds.), *Proceedings of the 17th International Conference on New Trends in Fatigue and Fracture*, https://doi.org/10.1007/978-3-319-70365-7_28

localized corrosion in virtue of its metallurgical design with low carbon content and significant amounts of Cr, Ni and Mo [5]. The 316L has a small thermal conductivity and a large coefficient of thermal expansion and it is prone to produce residual stress and deformation upon welding [6]. DSSs are compositionally formulated and thermomechanically processed to provide a two-phase microstructure with nearly equal proportions of ferrite and austenite. The outstanding properties of these alloys strongly depend on their phase balance. Welding of DSS yields a HAZ with a microstructure very different to the base metal due to elevated temperatures reached in this zone. Heating up of the alloy leads to a fully ferritic region with grain growth and precipitation of austenite during cooling. However, the time for the regeneration of austenite is not sufficient to restore the initial phase balance and the HAZ is prone to corrosion as the fillers for welding DSS are designed to enhanced formation of austenite during cooling [7]. Recent studies have shown some benefits when welding 304 ASS and 2205 DDS with the simultaneous application of an external magnetic field [8–11]. In principle, this practice induces an electromagnetic stirring (EMS) of the weld pool and affects the solidification mode. In the solid state, it generates vibration of the crystal structure and alters diffusion processes in short distances so that sensitization in the HAZ may be avoided [12]. This study is addressed to evaluate the effects on the microstructure and mechanical properties of the application of an external axial electromagnetic field of low intensity during welding plates of 2205 DSS and 316L ASS.

Materials and Experimental Methods

The plates employed in this study were 150 mm × 70 mm × 6.35 mm of 2205 DSS (UNS 31803) and 316L ASS (UNS S31603). Table 1 lists the chemical composition of the base materials along with the filler wire used for welding. The plates were machined to a single V-groove butt joint configuration (30° bevel, 1.5 mm root face and 2.5 mm root gap). Gas metal arc welding (GMAW) was performed in a sole pass with reverse polarity and a heat input of 1.2 kJ/mm (75% efficiency). An ER-2209 filler wire, 1.2 mm in diameter, fed at 160 mm/s was used along with the mixture 95% Ar + 3% N_2 + 2% O_2 as shielding gas flowing at 19 L/min. Welding was performed normal to the rolling direction of the plates at 3.6 mm/s with a stick out of 10 mm. The experimental setup for welding with the application of an external axial magnetic field is shown elsewhere [9, 10]. Briefly, it consists of a coil placed around the joint fed with an external power supply to

Table 1 Chemical composition of the base materials and filler wire employed (wt%)

Material	C	Mn	P	S	Si	Cr	Ni	Mo	N	Cu	Fe
2205	0.01	1.81	0.03	0	0.54	22.5	5.7	3.1	0.16	0.21	Bal.
316L	0.02	1.15	0.03	0	0.54	16.69	10.03	2.02	0.05	0.46	Bal.
ER-2209	0.012	1.75	0.02	0.01	0.5	23	8.8	3.2	0.14	0.1	Bal.

induce a magnetic field of 3 mT. This magnetic field interacts with the magnetic field inherent to the welding process and both generate an electromagnetic interaction of low intensity (EMILI).

The microstructural features were characterized in the optical microscope by preparing metallographic samples with standard procedures and chemical etching with Glyceregia reagent (15 cc HCl +10 cc Glycerol + 5 cc HNO_3). Vickers microhardness profiles were generated applying a load of 100 g during 15 s across transverse sections of the welds at the mid height of the welds. Three microhardness scannings were performed in each weld with a separation of 200 μm between line and punctual measurements. Dog bone shape specimens were machined from the base materials and welded joints to perform tensile testing with a cross head speed of 0.016 mm/s.

Results and Discussion

Figure 1 shows the characteristic microstructure in the rolling direction of the base materials in the as-received condition. The microstructure of the 2205 DSS, Fig. 1a, consists of elongated grains of austenite and δ-ferrite with an approximate fraction of 55 and 45%, respectively, approaching the ideal 50/50 ratio for the optimum mechanical and corrosion behavior. The 316L presents equiaxed grains of austenite, as seen in Fig. 1b, with a grain size of 15.11 ± 5.73 μm. It is also observed bands of residual δ-ferrite oriented in the rolling direction. The presence of this phase is due to segregation of chromium that promotes its precipitation during solidification and thermomechanical secondary processing [7].

The geometry of the welded joints is shown in the images of Fig. 2. Fully penetrated welds with no observable macro defects were obtained for both welding conditions. Chemical etching disclosed the profile of the weld bead and the HTHAZ of the 2205 DSS. The straight lines depict the initial configuration of the joint. Area measurements revealed that the size of the HTAZ of the 2205 DSS reduced from 6.77 to 4.04 mm^2 for the welds without and with magnetic field, respectively.

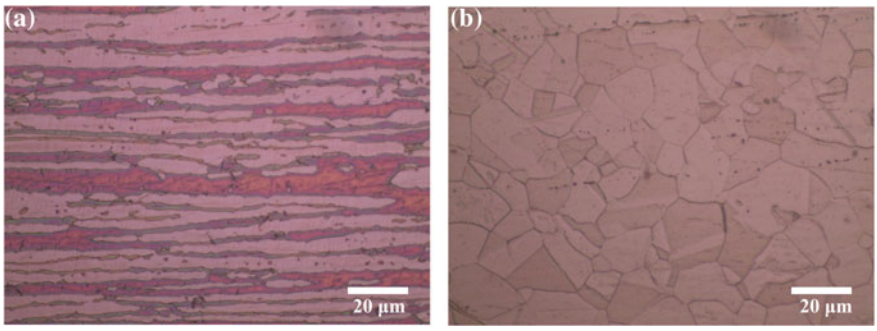

Fig. 1 Microstructure of the as-received base materials; **a** 2205 DSS and **b** 316L ASS

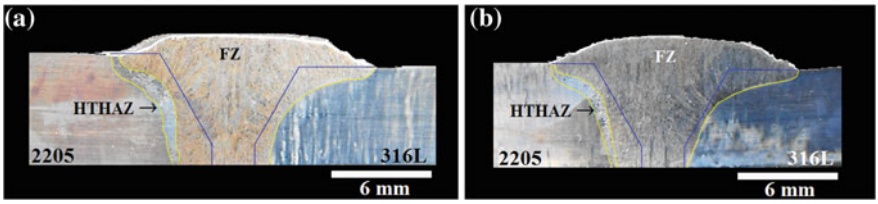

Fig. 2 Macrographs of the transverse views of the welded joints; **a** 0mT and **b** 3mT

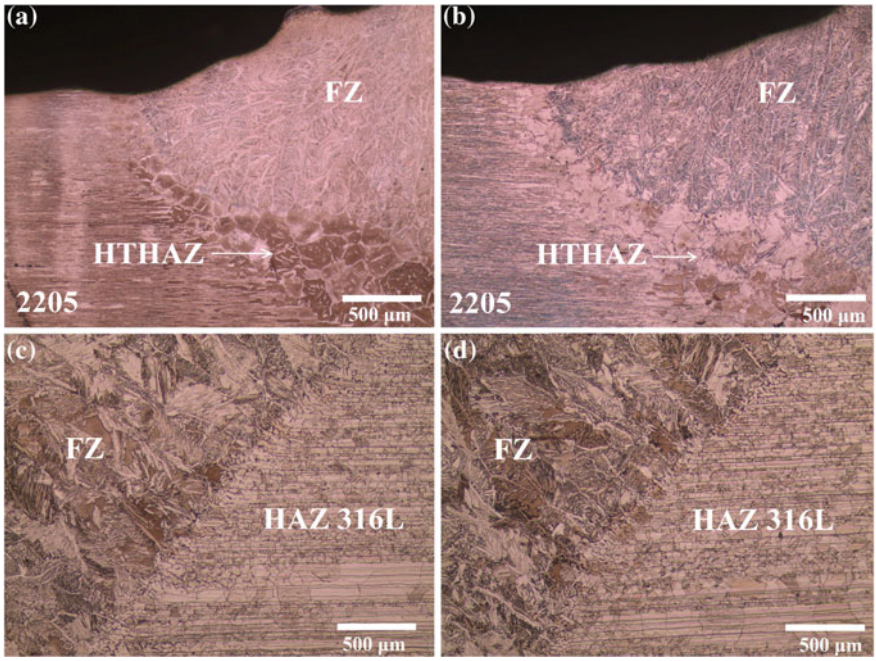

Fig. 3 Optical micrographs of the microstructure at the fusion line of the welds; **a–b** 2205 DSS and **c–d** 316L. Left 0 mT and right 3 mT

This effect is related to the EMS induced during welding [10, 13]. It promotes detachment of partially molten base material with its subsequent incorporation into the weld pool.

Figure 3 shows some details of the microstructure of the welds at the fusion line of every side of the welds. Figure 3a, b compare the side of the 2205 DSS without and with magnetic field, respectively. The microstructure in the HTHAZ for both welds is the typical one characterized by a ferritized region with austenite precipitating mainly in the limits of the coarse grains of ferrite. Measurement of the ferritic grain size, in equivalent locations in the HTHAZ, indicated a reduction of 10 µm in the average grain size and a reduction in the range size when using magnetic field.

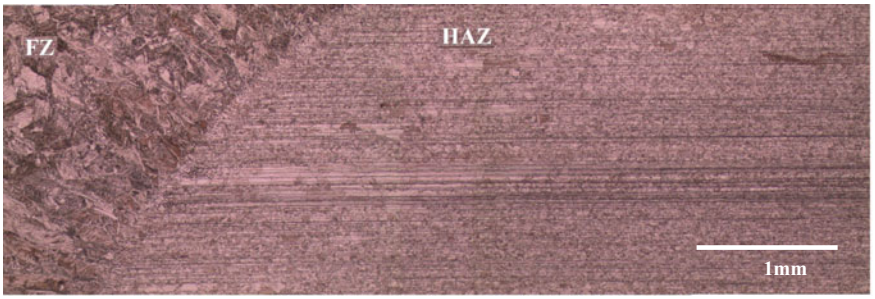

Fig. 4 Microstructural transitions of the weld at the side of the 316L ASS

A complex phenomenon involving magnetization and diffusion of substitutional elements may restrict coarsening of the ferritic matrix [14, 15]. In the fusion zone, the weld metal solidifies from the partially molten coarse ferritic grains of the HTHAZ growing toward the thermal gradient within the weld pool. The content of austenite in the weld metal is abundant owing to the high content of gammagenous elements in the metallurgical design of the filler wire. On the counter side, Figs. 3c, d compare the microstructure at the weld metal/316L ASS interface without and with magnetic field, respectively. This side of the welds is composed by a coarser microstructure in the fusion zone (as compared to the side of the 2205 DSS), a thin band of partially molten grains and the HAZ characterized by irregular grain growth. The bands of ferrite are clearly seen in the austenitic matrix. Figure 4 shows that grain growth in the HAZ occurred mostly at the mid height of the 316L plates where the concentration of stresses and ferrite caused by rolling of the plates is larger. In this zone, the size of the grains increased to an average value of 75 ± 29 μm. The presence of these large grains delimited the width of the HAZ up to 3 mm. Physical properties may revert to the previous state before cold-working caused by the welding thermal cycle. Such restoration results from two different processes that occur at elevated temperatures: recovery and recrystallization, may be followed by grain growth [16].

The variations in microhardness along the transverse section of the welds is shown in Fig. 5. In the side of the 2205 DSS, the results indicate that depending on the distance, the values are kept approximately constant at 258 ± 10 HV_{100}, lightly increasing in the HTHAZ to 272 ± 2 HV_{100} (closely to the as-received 2205 DSS). In the fusion zone, the values exhibited a slight decrease to 248 ± 7. Hardness of DSS is determined mainly by three factors; (i) nitrogen in solid solution in austenite. The content of 3% N_2 in the shielding gas compensates for the nitrogen loss during welding. (ii) The precipitation of hard secondary phases such as the nitrides, carbides and sigma phase may significantly increase hardness of DSS. (iii) The content of ferrite and its grain size. Ferrite is considered a strengthening phase in DSS and it is hardened by solution of alloying elements such as Cr and Mo, increasing the probability of precipitation of detrimental phases.

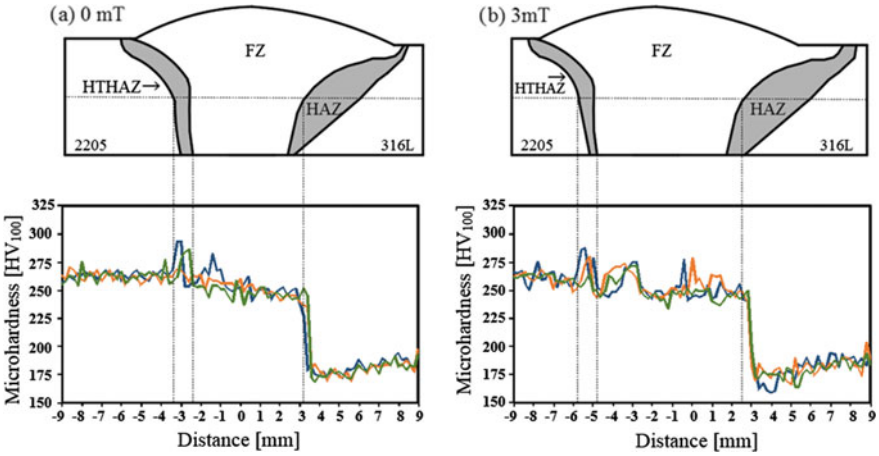

Fig. 5 Microhardness profiles along the different zones of the welds; **a** 0 mT and **b** 3 mT

The HTHAZ of 2205 DSS exhibited the highest microhardness values may be due to a combination of the following factors: (a) ferrite grains supersaturated with Cr and Mo and an increased ferrite content; (b) precipitation of hard Cr_2N; and (c) more nitrogen in solid solution in the primary austenite and the precipitation of Widmanstätten and acicular austenite [17]. The HAZ of the 316L ASS decreased its microhardness 18.5% (174 ± 8) as compared to the alloy in the as-received condition (215 ± 8).

Typical stress versus strain curves of the tensile test of the as-received base materials and welded joints are plotted in Fig. 6. The results of these tests are listed in Table 2. As expected, a higher mechanical strength is shown by the 2205 DSS whereas the 316L ASS exhibits significantly larger toughness. The welded joints essentially presented the same behavior independently of the welding condition with failure consistently occurring far away from the weld bead and beyond the HAZ. The mechanical strength of the dissimilar welds was slightly above the value of the 316L ASS with an elongation close to the 2205 DSS. These results mean that sound metallurgical dissimilar welds were obtained and an evaluation in corrosion properties is needed to further assess the effect of the application of the magnetic field during welding.

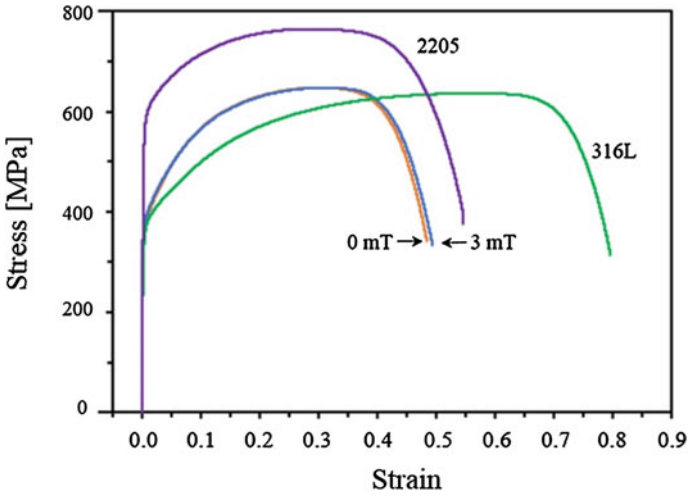

Fig. 6 Stress versus strain curves of the tensile specimens of the as-received base materials and welded joints

Table 2 Mechanical properties of base materials in the as-received condition and welded joints

Material	Yield stress (MPa)	Tensile strength (MPa)	Elongation %	HV_{100}
2205 DSS	558 ± 6.4	765 ± 1.5	55 ± 2	272 ± 9
316L ASS	344 ± 9.6	635 ± 9	81 ± 2.6	215 ± 8
Weld, 0 mT	358 ± 4	643 ± 5	50.7 ± 2	–
Weld, 3 mT	368 ± 15	644 ± 2	48.4 ± 2	–

Conclusion

Sound dissimilar 2205 DSS/316L ASS welded joints were obtained by the GMAW process with and without the application of an external axial magnetic field. In terms of microstructure, the use of the magnetic field during welding reduced the size of the HTHAZ of the DSS. The hardest region of the welded joints was the HTHAZ of the DSS irrespective of the welding condition. The thermal affection in the 316L ASS resulted in a moderate reduction in hardness and irregular grain growth at the mid height of the plates. Despite this effect, failure of the welds consistently occurred in the 316L ASS beyond the softened zone with a strength slightly above that of the base material in the as-received condition.

References

1. Mortezaie, A. and M. Shamanian, *An assessment of microstructure, mechanical properties and corrosion resistance of dissimilar welds between Inconel 718 and 310S austenitic stainless steel.* International Journal of Pressure Vessels and Piping, 2014. **116**(0): p. 37–46.
2. Verma, J., et al., *Microstructure, Mechanical and Intergranular Corrosion Behavior of Dissimilar DSS 2205 and ASS 316L Shielded Metal Arc Welds.* Transactions of the Indian Institute of Metals, 2017. **70**(1): p. 225–237.
3. Ibrahim, O.H., I.S. Ibrahim, and T.A.F. Khalifa, *Effect of Aging on the Toughness of Austenitic and Duplex Stainless Steel Weldments.* Journal of Materials Science & Technology, 2010. **26**(9): p. 810–816.
4. Moteshakker, A. and I. Danaee, *Microstructure and Corrosion Resistance of Dissimilar Weld-Joints between Duplex Stainless Steel 2205 and Austenitic Stainless Steel 316L.* Journal of Materials Science & Technology, 2016. **32**(3): p. 282–290.
5. Kianersi, D., A. Mostafaei, and A.A. Amadeh, *Resistance spot welding joints of AISI 316L austenitic stainless steel sheets: Phase transformations, mechanical properties and microstructure characterizations.* Materials & Design, 2014. **61**: p. 251–263.
6. Li, L.C., et al. *Effect of welding heat input on grain size and microstructure of 316L stainless steel welded Joint*. in *Applied mechanics and Materials*. 2013. Trans Tech Publ.
7. Lippold, J.C. and D.J. Kotecki, *Welding Metallurgy and Weldability af Stainless Steels*. 2011: Wiley India Pvt. Limited.
8. Curiel, F.F., et al., *Effect of magnetic field applied during gas metal arc welding on the resistance to localised corrosion of the heat affected zone in AISI 304 stainless steel.* Corrosion Science, 2011. **53**(7): p. 2393–2399.
9. García Rentería, M.A., et al., *Effect on the microstructure and mechanical properties of the electromagnetic stirring during GMA welding of 2205 DSS plates.* Materials Science Forum, 2013. **755**: p. 61–68.
10. García-Rentería, M., et al., *Improvement of localised corrosion resistance of AISI 2205 Duplex Stainless Steel joints made by gas metal arc welding under electromagnetic interaction of low intensity.* Applied Surface Science, 2014. **321**: p. 252–260.
11. García-Rentería, M., et al., *Effect of electromagnetic interaction during fusion welding of AISI 2205 duplex stainless steel on the corrosion resistance.* Applied Surface Science, 2017. **396**: p. 1187–1200.
12. Curiel, F.F., et al., *Transmission electron microscopy in the heat affected zone of an AISI 304 austenitic stainless steel welded with the application of a magnetic field of low intensity.* Materials Transactions, 2013. **54**(1): p. 122–125.
13. Villafuerte, J. and H. Kerr, *Electromagnetic Stirring and Grain-Refinement in Stainless-Steel GTA Welds.* Welding journal, 1990. **69**(1): p. S1-S13.
14. Liu, X.J., et al., *Effect of external magnetic field on thermodynamic properties and phase transitions in Fe-based alloys.* Journal of Alloys and Compounds, 2008. **459**(1–2): p. 169–173.
15. Liu, X.J., et al., *Effects of external magnetic field on the diffusion coefficient and kinetics of phase transformation in pure Fe and Fe–C alloys.* Calphad, 2011. **35**(1): p. 66–71.
16. Callister, W., *Materials Science and Engineering: An Introduction.*
17. Zhang, Z., et al., *Effects of nitrogen in shielding gas on microstructure evolution and localized corrosion behavior of duplex stainless steel welding joint.* Applied Surface Science, 2017. **404**: p. 110–128.